

Correlated inclusive $\Lambda\bar{\Lambda}$ production in e^+e^- annihilations at
 $\sqrt{s} \sim 10.5$ GeVCLEO Collaboration
(November 21, 2018)

Abstract

Using a 13.7 fb^{-1} sample of continuum two-jet $e^+e^- \rightarrow q\bar{q}$ events collected with the CLEO detector, we have searched for correlations between Λ and $\bar{\Lambda}$ particles, specifically in cases where the opening angle between the two particles is large and each has momentum >1 GeV/c. Such correlations may indicate the presence of baryon number conservation at the primary quark level. A previous CLEO study of $\Lambda_c\bar{\Lambda}_c$ correlations [5] indicated direct, associated production of primary charmed baryons Λ_c : $e^+e^- \rightarrow c\bar{c} \rightarrow \Lambda_c\bar{\Lambda}_c$. That effect was not observed in Monte Carlo simulations. Our current search for similar direct, associated production of Λ baryons at the primary quark level ($e^+e^- \rightarrow s\bar{s} \rightarrow \Lambda\bar{\Lambda}$, e.g.) qualitatively indicates a similar effect, although it relies on a Monte Carlo dependent subtraction of background $\Lambda\bar{\Lambda}$ production (based on the default JETSET 7.4 event generator).

Z. Metreveli,¹ K.K. Seth,¹ A. Tomaradze,¹ P. Zwebber,¹ S. Ahmed,² M. S. Alam,² L. Jian,² M. Saleem,² F. Wappler,² E. Eckhart,³ K. K. Gan,³ C. Gwon,³ T. Hart,³ K. Honscheid,³ D. Hufnagel,³ H. Kagan,³ R. Kass,³ T. K. Pedlar,³ J. B. Thayer,³ T. Wilksen,³ M. M. Zoeller,³ H. Muramatsu,⁴ S. J. Richichi,⁴ H. Severini,⁴ P. Skubic,⁴ S.A. Dytman,⁵ J.A. Mueller,⁵ S. Nam,⁵ V. Savinov,⁵ S. Chen,⁶ J. W. Hinson,⁶ J. Lee,⁶ D. H. Miller,⁶ V. Pavlunin,⁶ E. I. Shibata,⁶ I. P. J. Shipsey,⁶ D. Cronin-Hennessy,⁷ A.L. Lyon,⁷ C. S. Park,⁷ W. Park,⁷ E. H. Thorndike,⁷ T. E. Coan,⁸ Y. S. Gao,⁸ F. Liu,⁸ Y. Maravin,⁸ I. Narsky,⁸ R. Stroynowski,⁸ M. Artuso,⁹ C. Boulahouache,⁹ K. Bukin,⁹ E. Dambasuren,⁹ K. Khroustalev,⁹ G. C. Moneti,⁹ R. Mountain,⁹ R. Nandakumar,⁹ T. Skwarnicki,⁹ S. Stone,⁹ J.C. Wang,⁹ A. H. Mahmood,¹⁰ S. E. Csorna,¹¹ I. Danko,¹¹ Z. Xu,¹¹ G. Bonvicini,¹² D. Cinabro,¹² M. Dubrovin,¹² S. McGee,¹² A. Bornheim,¹³ E. Lipeles,¹³ S. P. Pappas,¹³ A. Shapiro,¹³ W. M. Sun,¹³ A. J. Weinstein,¹³ G. Masek,¹⁴ H. P. Paar,¹⁴ R. Mahapatra,¹⁵ R. A. Briere,¹⁶ G. P. Chen,¹⁶ T. Ferguson,¹⁶ G. Tatishvili,¹⁶ H. Vogel,¹⁶ N. E. Adam,¹⁷ J. P. Alexander,¹⁷ K. Berkelman,¹⁷ F. Blanc,¹⁷ V. Boisvert,¹⁷ D. G. Cassel,¹⁷ P. S. Drell,¹⁷ J. E. Duboscq,¹⁷ K. M. Ecklund,¹⁷ R. Ehrlich,¹⁷ R. S. Galik,¹⁷ L. Gibbons,¹⁷ B. Gittelman,¹⁷ S. W. Gray,¹⁷ D. L. Hartill,¹⁷ B. K. Heltsley,¹⁷ L. Hsu,¹⁷ C. D. Jones,¹⁷ J. Kandaswamy,¹⁷ D. L. Kreinick,¹⁷ A. Magerkurth,¹⁷ H. Mahlke-Krüger,¹⁷ T. O. Meyer,¹⁷ N. B. Mistry,¹⁷ E. Nordberg,¹⁷ J. R. Patterson,¹⁷ D. Peterson,¹⁷ J. Pivarski,¹⁷ D. Riley,¹⁷ A. J. Sadoff,¹⁷ H. Schwarthoff,¹⁷ M. R. Shepherd,¹⁷ J. G. Thayer,¹⁷ D. Uner,¹⁷ B. Valant-Spaight,¹⁷ G. Viehhauser,¹⁷ A. Warburton,¹⁷ M. Weinberger,¹⁷ S. B. Athar,¹⁸ P. Avery,¹⁸ L. Brevva-Newell,¹⁸ V. Potlia,¹⁸ H. Stoeck,¹⁸ J. Yelton,¹⁸ G. Brandenburg,¹⁹ A. Ershov,¹⁹ D. Y.-J. Kim,¹⁹ R. Wilson,¹⁹ K. Benslama,²⁰ B. I. Eisenstein,²⁰ J. Ernst,²⁰ G. D. Gollin,²⁰ R. M. Hans,²⁰ I. Karliner,²⁰ N. Lowrey,²⁰ M. A. Marsh,²⁰ C. Plager,²⁰ C. Sedlack,²⁰ M. Selen,²⁰ J. J. Thaler,²⁰ J. Williams,²⁰ K. W. Edwards,²¹ R. Ammar,²² D. Besson,²² M. Cervantes,²² X. Zhao,²² S. Anderson,²³ V. V. Frolov,²³ Y. Kubota,²³ S. J. Lee,²³ S. Z. Li,²³ R. Poling,²³ A. Smith,²³ C. J. Stepaniak,²³ and J. Urheim²³

¹Northwestern University, Evanston, Illinois 60208

²State University of New York at Albany, Albany, New York 12222

³Ohio State University, Columbus, Ohio 43210

⁴University of Oklahoma, Norman, Oklahoma 73019

⁵University of Pittsburgh, Pittsburgh, Pennsylvania 15260

⁶Purdue University, West Lafayette, Indiana 47907

⁷University of Rochester, Rochester, New York 14627

⁸Southern Methodist University, Dallas, Texas 75275

⁹Syracuse University, Syracuse, New York 13244

¹⁰University of Texas - Pan American, Edinburg, Texas 78539

¹¹Vanderbilt University, Nashville, Tennessee 37235

¹²Wayne State University, Detroit, Michigan 48202

¹³California Institute of Technology, Pasadena, California 91125

¹⁴University of California, San Diego, La Jolla, California 92093

¹⁵University of California, Santa Barbara, California 93106

¹⁶Carnegie Mellon University, Pittsburgh, Pennsylvania 15213

¹⁷Cornell University, Ithaca, New York 14853

¹⁸University of Florida, Gainesville, Florida 32611

¹⁹Harvard University, Cambridge, Massachusetts 02138

²⁰University of Illinois, Urbana-Champaign, Illinois 61801

²¹Carleton University, Ottawa, Ontario, Canada K1S 5B6
and the Institute of Particle Physics, Canada M5S 1A7

²²University of Kansas, Lawrence, Kansas 66045

²³University of Minnesota, Minneapolis, Minnesota 55455

I. INTRODUCTION

At $\sqrt{s} \sim 10$ GeV, below the threshold for $e^+e^- \rightarrow B\bar{B}$, particle production in e^+e^- annihilation occurs in a largely low- Q^2 , non-perturbative regime. Fragmentation models are therefore used to describe the process $e^+e^- \rightarrow \text{hadrons}$. Computer codes such as JETSET [1] have been extremely successful at matching experimental results on inclusive particle production, multiplicities and angular distributions, both qualitatively and, to a large degree, quantitatively. Compensation of baryon number is one of the more subtle aspects of particle fragmentation modeling. One obvious question is whether baryon compensation occurs locally (e.g., small opening angle between baryon and antibaryon) or globally (large opening angles). In the case when a baryon is produced in the first step of fragmentation ($e^+e^- \rightarrow c\bar{c}$; $c \rightarrow \Lambda_c$, e.g.), it is possible that both baryon and flavor quantum numbers will be compensated in the opposite hemisphere¹ (e.g., $e^+e^- \rightarrow c\bar{c}$; $c \rightarrow \Lambda_c$; $\bar{c} \rightarrow \bar{\Lambda}_c$). However, in models in which the primary quark and anti-quark fragment entirely independently of each other, no such correlations are expected.

Previous LEP studies [2–4] of $\Lambda\bar{\Lambda}$ production at $\sqrt{s}=90$ GeV found that in events containing both a Λ and a $\bar{\Lambda}$, the two particles tend to be produced with small opening angles between them. Those analyses also discriminated between different models of $\Lambda\bar{\Lambda}$ production. It was found in the DELPHI and ALEPH analyses that the JETSET string fragmentation event generator gave excellent agreement with data when the “popcorn” control parameter ρ was set to 0.5; the OPAL analysis favored slightly higher values of ρ . (In the default CLEO Monte Carlo event generator, we have used $\rho=0.5$.) In those previous studies, no statistically significant signal for correlated opposite-hemisphere, primary ($\Lambda\bar{\Lambda}$) production was found.

A previous CLEO study [5] of charmed baryons sought to discriminate between independent vs. correlated fragmentation models. Assuming that primary particles fragment independently, then the number of times that we find a Λ_c baryon opposite a $\bar{\Lambda}_c$ antibaryon in an event (denoted “ $\Lambda_c|\bar{\Lambda}_c$ ”), scaled to the total number of observed $\bar{\Lambda}_c$ (denoted “ $\frac{(\Lambda_c|\bar{\Lambda}_c)}{\bar{\Lambda}_c}$ ”), should be equal to the number of times that we find a Λ_c baryon opposite any other anti-charmed hadron \bar{H}_c scaled to the total number of observed anti-charmed hadrons ($\frac{(\Lambda_c|\bar{H}_c)}{\bar{H}_c}$). It was found that, given a $\bar{\Lambda}_c$ (reconstructed in five different decay modes), a Λ_c is observed in the opposite hemisphere (0.72 ± 0.11)% of the time (not corrected for efficiency). By contrast, given a \bar{D} , a Λ_c is observed in the opposite hemisphere only (0.21 ± 0.02)% of the time. Normalized to the total number of either $\bar{\Lambda}_c$ or \bar{D} “tags”, that study concluded that it is $3.52 \pm 0.45 \pm 0.42$ times more likely to find a Λ_c opposite

¹We define two particles to be “opposite hemisphere” if their opening angle exceeds 90 degrees. This definition is therefore disconnected from momentum flow in the remainder of the event and is only indirectly related to such standard parameters as thrust, sphericity, etc. As is demonstrated in the text, most Λ baryons emerge either very close to, or directly opposite, the anti- Λ studied, so the separation of an event into hemispheres is at least approximately valid.

a $\bar{\Lambda}_c$ than opposite a \bar{D} meson. This enhancement is not produced in the default JETSET 7.4 $e^+e^- \rightarrow c\bar{c}$ Monte Carlo simulation.

As a straightforward extension of that analysis, we can search for similar correlations between primary Λ and $\bar{\Lambda}$ baryons. In this case, the correlation is obscured by the fact that, unlike Λ_c baryons, Λ 's produced in e^+e^- annihilations do not necessarily contain the primary quarks, and will be produced copiously in fragmentation, as well as in weak decays of charmed baryons. In our current analysis, the production of $(\Lambda|\bar{\Lambda})$ through fragmentation is modeled using the JETSET 7.4 event generator combined with a GEANT-based [6] simulation of our detector. The “feeddown” contribution from correlated primary $(\Lambda_c|\bar{\Lambda}_c)$ production ($\Lambda_c \rightarrow \Lambda|\bar{\Lambda}_c \rightarrow \bar{\Lambda}$) is evaluated from the data itself.

For this study, Λ_c^+ 's are fully reconstructed in the decay modes $\Lambda_c^+ \rightarrow pK^-\pi^+$, $\Lambda_c^+ \rightarrow pK_S^0$, $\Lambda_c^+ \rightarrow \Lambda\pi^+$, $\Lambda_c^+ \rightarrow \Lambda\pi^+\pi^-\pi^+$, $\Lambda_c^+ \rightarrow pK_S^0\pi^+\pi^-$,² and partially reconstructed through $\Lambda_c^+ \rightarrow \Lambda X$. Λ baryons are reconstructed in $\Lambda \rightarrow p\pi^-$.

II. APPARATUS AND EVENT SELECTION

This analysis was performed using the CLEO II and the upgraded CLEO II.V detectors operating at the Cornell Electron Storage Ring (CESR) at center-of-mass energies $\sqrt{s} = 10.52\text{--}10.58$ GeV. The event sample used for this measurement is comprised of 9.2 fb^{-1} of data collected at the $\Upsilon(4S)$ resonance and 4.6 fb^{-1} of data collected about 60 MeV below the $\Upsilon(4S)$ resonance. Approximately 20×10^6 continuum $c\bar{c}$ events³ are included in this sample.

For 4.6 fb^{-1} of the data used for this analysis (“CLEO-II” data [7]), measurements of charged particle momenta were made with three nested coaxial drift chambers consisting of 6, 10, and 51 layers, respectively. In a subsequent upgrade (“CLEO-II.V” [8], corresponding to the remaining data used for this analysis), the innermost tracking chamber was replaced with a high-precision silicon detector, and the gas in the main tracking volume was changed to provide better cell resolution and improved specific ionization (dE/dx) resolution [9]. The entire tracking system fills the volume from $r=3$ cm to $r=1$ m, with r the radial coordinate relative to the beam (\hat{z}) axis. This system is very efficient ($\epsilon \geq 98\%$) for detecting tracks that have transverse momenta (p_T) relative to the beam axis greater than 200 MeV/c, and that are contained within the good fiducial volume of the drift chamber ($|\cos\theta_Z| < 0.94$, with θ_Z defined as the polar angle relative to the beam axis). This system achieves a momentum resolution of $(\delta p/p)^2 = (0.0015p)^2 + (0.005)^2$ (p is the momentum, measured in GeV/c). Pulse-height measurements in the main drift chamber provide specific ionization resolution of 5.0% (CLEO II.V) or 5.5% (CLEO II) for Bhabha events, giving excellent K/π separation for tracks with momenta up to 700 MeV/c and separation of order 2σ in the relativistic rise region above 2.5 GeV/c. Outside the central tracking chambers are plastic scintillation counters, which are used as a fast element in the trigger system and also provide particle identification information from time-of-flight measurements.

Beyond the time-of-flight system is the electromagnetic calorimeter, consisting of 7800 thallium-doped CsI crystals. The central “barrel” region of the calorimeter covers about 75% of the solid angle and has an energy resolution which is empirically found to follow:

²Charge conjugation is implicit.

³Corresponding to approximately 20×10^6 $u\bar{u}$, 5×10^6 $d\bar{d}$, and 5×10^6 $s\bar{s}$ events, respectively.

$$\frac{\sigma_E}{E}(\%) = \frac{0.35}{E^{0.75}} + 1.9 - 0.1E; \quad (1)$$

E is the shower energy in GeV. This parameterization includes noise effects, and translates to an energy resolution of about 4% at 100 MeV and 1.2% at 5 GeV. Two end-cap regions of the crystal calorimeter extend solid angle coverage to about 95% of 4π , although energy resolution is not as good as that of the barrel region. The tracking system, time-of-flight counters, and calorimeter are all contained within a superconducting coil operated at 1.5 Tesla. An iron flux return interspersed with proportional tubes used for muon detection are located immediately outside the coil and in the two end-cap regions.

Primary proton, kaon or pion charged track candidates must pass the following restrictions:

(a) The track must pass a 99% probability criterion for its assumed particle identification, based on the associated charged track's specific ionization measured in the drift chamber.

(b) The track must have momentum greater than 100 MeV/c.

Each reconstructed charmed hadron must have momentum greater than 2.3 GeV/c to ensure that there is no contamination from B -meson decays to charm.

III. DATA ANALYSIS

A. Production Ratios

We define the single-tag yield to be the number of reconstructed events containing one particular hadron H . This yield is typically determined by fitting a double-Gaussian signal atop a smooth, low-order polynomial background function. The number of double-tags is defined as the number of events in which two specific particles are both reconstructed, separated by less than 90 degrees ($H_1\overline{H}_2$; ‘same-hemisphere’) or greater than 90 degrees ($H_1|H_2$; ‘opposite hemisphere’).⁴

To suppress possible contributions from $e^+e^- \rightarrow \Upsilon(4S) \rightarrow B\overline{B}$, with subsequent decays such as $\overline{B} \rightarrow \Xi_c(\rightarrow \Lambda X)\overline{\Lambda}X$, we have imposed a minimum momentum requirement $p_\Lambda > 1.0$ GeV/c. Decays of B -mesons should generally produce lower momentum Λ and $\overline{\Lambda}$; $B\overline{B}$ events are also likely to have different $\Lambda\overline{\Lambda}$ production dynamics compared to $\Lambda\overline{\Lambda}$ production resulting from direct e^+e^- annihilations. (The requirement $p_\Lambda > 1.0$ GeV/c is “standard” in other continuum Lambda studies as well [5,10,11].) In order to check whether there is $B\overline{B}$ contamination of the $\Lambda\overline{\Lambda}$ data sample, we compare our $\Lambda\overline{\Lambda}$ yield derived from data taken on the $\Upsilon(4S)$ resonance with the $\Lambda\overline{\Lambda}$ yield obtained using data taken on the continuum below the resonance. We expect these yields to be in the ratio of the integrated luminosities of the two samples, corrected for the $1/s$ dependence of the continuum cross-section, if there is no $B\overline{B}$ contamination (these two effects give an expected ratio of 2.01 for our data). Requiring $p_\Lambda > 1.0$ GeV/c, the yield of same-hemisphere $\Lambda\overline{\Lambda}$ pairs on the $\Upsilon(4S)$ resonance (5610.4 ± 79.1) compared to the yield for the continuum (2815.2 ± 56.1) is, indeed, consistent (at the 2σ level) with this ratio. Opposite hemisphere yields (4962.8 ± 78.8 and 2398.9 ± 54.4 , respectively) are similarly consistent with an exclusively continuum origin of our $\Lambda\overline{\Lambda}$ sample. For maximal statistics, we use our entire sample for the subsequent analysis, and discuss residual $B\overline{B}$ contamination effects later in this document.

⁴We use the notation “ H_1H_2 ” (without a vertical bar) to indicate a generic correlation event in which the two particles may be found in either hemisphere relative to each other.

The yields of $\Lambda_c|\overline{\Lambda}_c$, $\Lambda_c|\overline{\Lambda}$, $\Lambda|\overline{\Lambda}$ (opposite hemisphere) and $\Lambda\overline{\Lambda}$ (same hemisphere) double-tags are extracted from two-dimensional invariant mass plots, shown in Figures 1, 2, and 3, and 4, respectively. The total correlated double-tag yield is first determined by fitting one-dimensional projections of the two-dimensional plots. Consider, for example Fig. 1. We take one-dimensional projections of three slices in the candidate $\overline{\Lambda}_c$ recoil invariant mass: the $\overline{\Lambda}_c$ signal region: ($|M_{recoil} - 2.286| < 0.03 \text{ GeV}/c^2$) and the two $\overline{\Lambda}_c$ sideband regions: ($0.04 < |M_{recoil} - 2.286| < 0.07 \text{ GeV}/c^2$). We then subtract the fitted Λ_c yields from the $\overline{\Lambda}_c$ sidebands from that of the signal region. In performing these fits, the double-Gaussian signal shapes are constrained using the parameters determined from fits to the single-tag sample. We also perform a single fit in two dimensions to extract the signal yields. In this latter fit, a two-dimensional Gaussian signal is used to parametrize the peak region, two single Gaussians are used to fit the “ridges” away from the peak region (corresponding to true signals along one axis in association with combinatoric background on the other axis) and a two-dimensional, smooth polynomial is used to parametrize the background. The two procedures result in consistent signal yields; the yields presented in Table I result from application of the second procedure.

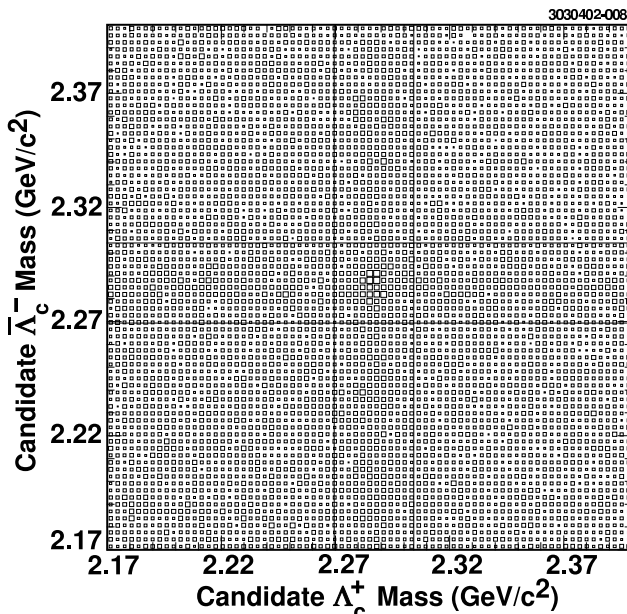


FIG. 1. Double-tag invariant mass of Λ_c candidates plotted vs. invariant mass of $\overline{\Lambda}_c$ candidates ($\Lambda_c\overline{\Lambda}_c$) from data. Shown is the sum of the modes: $\Lambda_c^+ \rightarrow pK^-\pi^+$, $\Lambda_c^+ \rightarrow pK_S^0$, $\Lambda_c^+ \rightarrow \Lambda\pi^+$, $\Lambda_c^+ \rightarrow \Lambda\pi^+\pi^-\pi^+$, and $\Lambda_c^+ \rightarrow pK_S^0\pi^+\pi^-$ (and their charge conjugates, in the case of $\overline{\Lambda}_c$ reconstruction).

Table I summarizes yields in both data and Monte Carlo simulations of comparable size. No detection efficiency corrections have been applied. The number of observed inclusive, single-tag particles is presented, in addition to the number of same hemisphere double-tags ($\Lambda\overline{\Lambda}$), opposite-hemisphere double-tags ($\Lambda|\overline{\Lambda}$), and the rate of double-tags per single-tag ($(\Lambda|\overline{\Lambda})/\Lambda$). Where appropriate, differences of data ratios minus Monte Carlo ratios are given to allow direct comparisons (column 4 in the Table).

Comparing the Monte Carlo vs. data yields in Table I, we note:

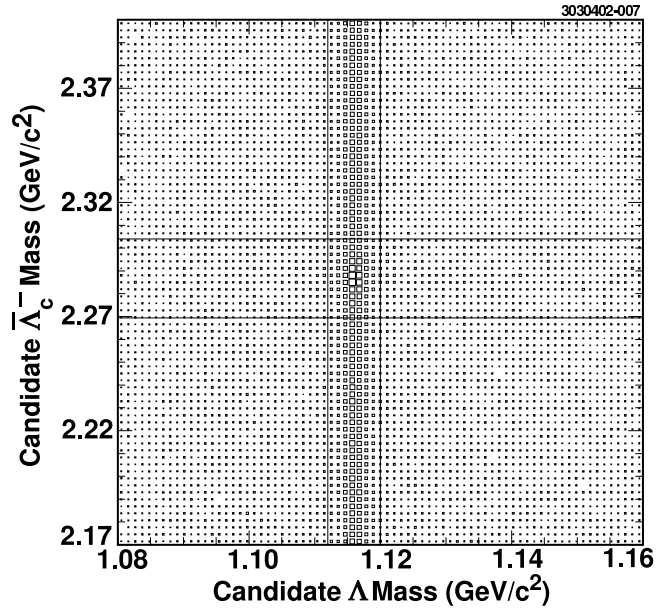


FIG. 2. Double-tag plot of $\Lambda|\bar{\Lambda}_c$ (plus charge conjugate) from data. The $\bar{\Lambda}_c$ is selected as in the previous Figure; the Λ is reconstructed in $\Lambda \rightarrow p\pi^-$.

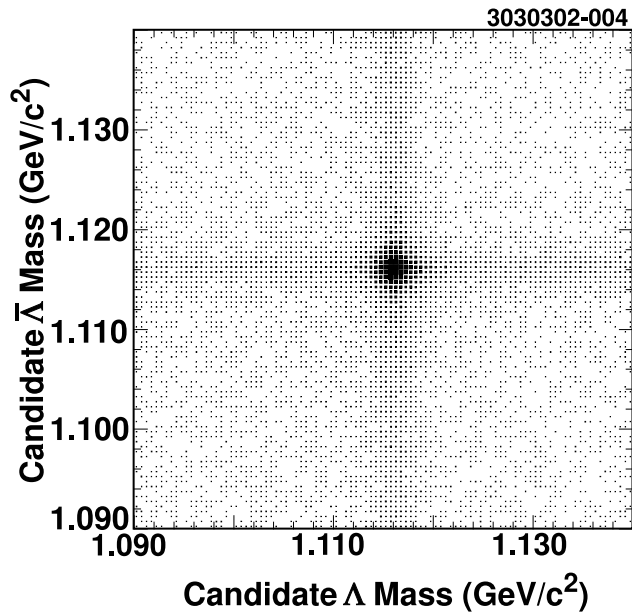


FIG. 3. Double-tag plot of $\Lambda|\bar{\Lambda}$ (opposite hemisphere) for data.

TABLE I. Yields in data vs. Monte Carlo simulations. The data are drawn from a sample of $\sim 50 \times 10^6$ hadronic events ($\sim 2/3$ on- $\Upsilon(4S)$ events plus $\sim 1/3$ taken on the continuum below the $\Upsilon(4S)$); the MC is drawn from a sample of $\sim 60 \times 10^6$ exclusively continuum events generated by JETSET 7.4, fully simulated in our CLEO detector and reconstructed using the same algorithms as applied to data. Derivation of final results (specifically, the derivation of the $\Lambda|\bar{\Lambda}$ ($q\bar{q}$) signal yield and evaluation of the non-primary $\Lambda|\bar{\Lambda}$ (np) and charmed-baryon $\Lambda|\bar{\Lambda}$ ($c\bar{c}$) backgrounds) are discussed in detail in the text. The difference (Data-Monte Carlo) in the fourth column is shown only for the yield ratios, which are sample-size independent.

	Data	Monte Carlo	Data - MC
$\Lambda_c + \bar{\Lambda}_c$ ($p > 2.3$ GeV/c)	83955 ± 1852	92731 ± 810	
$(\Lambda + \bar{\Lambda})$ (ON-4S, $p > 1$ GeV/c)	491087 ± 822		
$(\Lambda + \bar{\Lambda})$ (Continuum, $p > 1$ GeV/c)	236162 ± 575	973657 ± 1121	
$\Lambda + \bar{\Lambda}$ (total, $p > 1$ GeV/c)	727249 ± 1003	973657 ± 1121	
$(\Lambda_c \bar{\Lambda}_c)$	323.6 ± 39.3	97.2 ± 40.4	
$(\Lambda_c \bar{\Lambda}) + (\bar{\Lambda}_c \Lambda)$	1470.6 ± 74.1	695.8 ± 67.1	
$(\Lambda_c \bar{\Lambda}) + (\bar{\Lambda}_c \Lambda)$	249.4 ± 26.2	210.7 ± 28.9	
$(\Lambda \bar{\Lambda})$	7361.8 ± 95.7	6519 ± 91.0	
$(\Lambda\bar{\Lambda})$	8425.6 ± 97.0	11394.9 ± 112.4	
$(\Lambda\Lambda)$	28.6 ± 15.3	36.4 ± 12.4	
$(\Lambda \Lambda)$	239.8 ± 37.2	401.0 ± 33.9	
$(\Lambda_c \bar{\Lambda}_c)/(\Lambda_c + \bar{\Lambda}_c)$ ($\times 10^{-3}$)	3.91 ± 0.47	1.05 ± 0.44	2.86 ± 0.64
$(\bar{\Lambda}_c \Lambda + \Lambda_c \bar{\Lambda})/(\Lambda + \bar{\Lambda})$ ($\times 10^{-4}$)	3.43 ± 0.36	2.16 ± 0.30	1.27 ± 0.46
$(\bar{\Lambda}_c \Lambda + \Lambda_c \bar{\Lambda})/(\Lambda + \bar{\Lambda})$ ($\times 10^{-4}$)	20.2 ± 1.0	7.1 ± 0.7	13.1 ± 1.2
$(\Lambda \bar{\Lambda})/(\Lambda + \bar{\Lambda})$ ($\times 10^{-2}$)	1.01 ± 0.01	0.67 ± 0.01	0.34 ± 0.02
$(\Lambda\bar{\Lambda})/(\Lambda + \bar{\Lambda})$ ($\times 10^{-2}$)	1.16 ± 0.01	1.17 ± 0.01	-0.01 ± 0.01
$(\Lambda\Lambda)/(\Lambda + \bar{\Lambda})$ ($\times 10^{-5}$)	3.93 ± 2.10	3.73 ± 1.27	0.20 ± 2.45
$(\Lambda \Lambda)/(\Lambda + \bar{\Lambda})$ ($\times 10^{-5}$)	33.0 ± 5.1	41.2 ± 4.1	-8.2 ± 6.6
Maximum $(\Lambda \bar{\Lambda})$ (np) background	4820 ± 82	6519 ± 91	
Tagged MC $(\Lambda \bar{\Lambda})$ from $(\Lambda_c \bar{\Lambda}_c)$ evts.		477 ± 22	
$(\Lambda \bar{\Lambda})$ (np) estimate, corrected	4466 ± 84	6042 ± 93	
Maximum $(\Lambda \bar{\Lambda})$ ($c\bar{c}$) background	1671 ± 221		
$(\Lambda \bar{\Lambda})$ ($q\bar{q}$), max. bkgnds.	872 ± 288		
$(\Lambda \bar{\Lambda}_c)$ evts. from $(\bar{D}\Lambda) \Lambda_c$	200 ± 34	169 ± 13 (tagged)	
$(\Lambda \bar{\Lambda})$ ($c\bar{c}$), corrected for $((D\Lambda) \Lambda_c)$	1251 ± 223		
$(\Lambda \bar{\Lambda})$ ($q\bar{q}$), $(\Lambda \bar{\Lambda})$ ($c\bar{c}$) corrected	1290 ± 371		
$(\Lambda \bar{\Lambda})$ ($q\bar{q}$), ALL corrections	1643 ± 372		

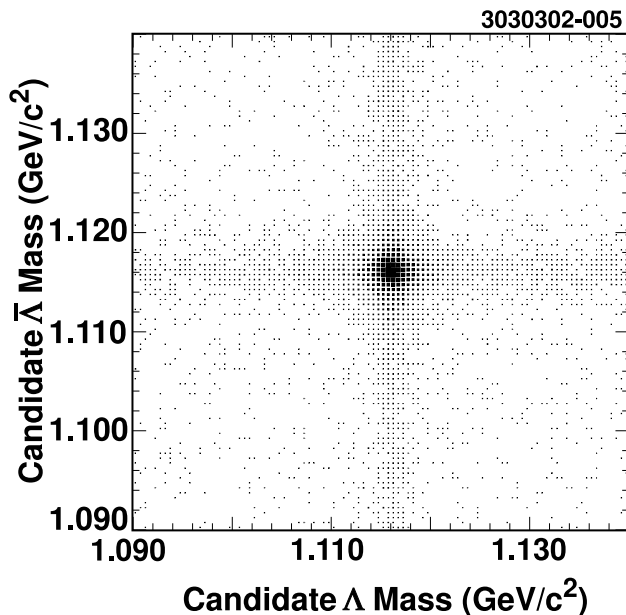


FIG. 4. Double-tag plot of $\Lambda\bar{\Lambda}$ (same hemisphere) for data.

1. There is an enhancement, in data, of the number of $\Lambda_c|\bar{\Lambda}_c$ per event, relative to Monte Carlo (top line of Table I). This correlated production was the subject of our previous paper [5], and was interpreted as evidence for correlated production of charmed baryons from primary quarks.⁵
2. There is an enhancement in the $\Lambda_c|\bar{\Lambda}$ yield in data relative to Monte Carlo. This can largely be attributed to the aforementioned correlated $\Lambda_c|\bar{\Lambda}_c$ production, in which the decay $\bar{\Lambda}_c \rightarrow \bar{\Lambda}$ results in a $\bar{\Lambda}$ in the hemisphere opposite the Λ_c . Such events will also result from cases in which charm is compensated by a meson rather than a baryon: $\Lambda_c K|\bar{\Lambda}\bar{D}$.
3. In four-baryon events (events with either $\Lambda\Lambda$ or $\Lambda|\Lambda$), both data and Monte Carlo show a preference for $\Lambda|\Lambda$ over $\Lambda\Lambda$. This is consistent with a model in which two $\Lambda\bar{\Lambda}$ pairs, each with $\cos\theta_{\Lambda\bar{\Lambda}} \rightarrow 1$, are created such that one $\Lambda\bar{\Lambda}$ pair is directly opposite the second $\Lambda\bar{\Lambda}$ pair. The actual source of these events, although interesting, is not the focus of our current effort and its discussion will be deferred until further study. For now, we note that to the extent that $\Lambda\bar{\Lambda}\Lambda\bar{\Lambda}$ events are contributing to both $\Lambda\Lambda$ and $\Lambda\bar{\Lambda}$ samples, statistical consistency between Monte Carlo and data in the relative ratios of $(\Lambda\Lambda)/\Lambda$ and $(\Lambda|\Lambda)/\Lambda$ indicates that Monte Carlo simulations model such events reasonably well.
4. The number of same-hemisphere $\Lambda\bar{\Lambda}$ correlations, divided by the total number of single-tag Λ particles, gives ratios, respectively for data and for Monte Carlo:

⁵We have loosened the Λ_c selection requirements for this analysis relative to our previous analysis. This results in approximately 20%(44%) larger single-tag(double-tag) Λ_c reconstruction efficiency.

$$\text{DATA} : \frac{(\Lambda\bar{\Lambda})}{(\Lambda + \bar{\Lambda})} = (1.16 \pm 0.01)\%$$

$$\text{MONTE CARLO} : \frac{(\Lambda\bar{\Lambda})}{(\Lambda + \bar{\Lambda})} = (1.17 \pm 0.01)\%$$

which are in excellent agreement. This agreement gives us confidence that the Monte Carlo simulation provides an adequate model of the non-primary component, which is expected to dominate the small opening angle sample.⁶

5. By contrast, the opposite hemisphere yields:

$$\text{DATA} : \frac{(\Lambda|\bar{\Lambda})}{(\Lambda + \bar{\Lambda})} = (1.01 \pm 0.01)\%$$

$$\text{MONTE CARLO} : \frac{(\Lambda|\bar{\Lambda})}{(\Lambda + \bar{\Lambda})} = (0.67 \pm 0.01)\%$$

indicate large opening-angle $\Lambda|\bar{\Lambda}$ production in data at a rate 50% greater than the Monte Carlo simulation.⁷ The total number of observed $\Lambda|\bar{\Lambda}$ events should arise primarily from three sources:

- a) our signal of interest: direct primary production in $e^+e^- \rightarrow q\bar{q}$ ($q = u, d, \text{ or } s$) events by a mechanism similar to that which leads to the observed $\Lambda_c|\bar{\Lambda}_c$ enhancement (designated “ $(\Lambda|\bar{\Lambda})(q\bar{q})$ ”);
- b) $\Lambda|\bar{\Lambda}$ events due to feeddown from $e^+e^- \rightarrow c\bar{c} \rightarrow \Lambda_c\bar{\Lambda}_c$, with: $\Lambda_c \rightarrow (\Lambda|\bar{\Lambda}_c \rightarrow \bar{\Lambda})$ (designated “ $\Lambda|\bar{\Lambda}(c\bar{c})$ ”) and
- c) non-primary Λ baryons which do not contain a primary light quark and are not Λ_c decay products (designated “ $\Lambda|\bar{\Lambda}(\text{np})$ ”).

Generally, we will use “fragmentation”, or “non-primary” to denote particles not containing primary quarks and particles which are not direct weak decay products of charmed hadrons. In contrast to a) and b), fragmentation will lead to events containing both Λ and $\bar{\Lambda}$ in the same-hemisphere, as well as opposite-hemispheres. We now outline our subtraction of these background components.

⁶We do not include among the non-primary hadrons the feed-down Λ decay products of Λ_c , since they include part of the primary hadron.

⁷It was found that setting the JETSET parameter $\rho=0.6$, as suggested by OPAL, resulted in a larger $\Lambda|\bar{\Lambda}$ yield, but also produced a substantial deficit in the same-hemisphere Monte Carlo $\Lambda\bar{\Lambda}$ yield compared to data, and thus gave a considerably inferior match to the $\Lambda\bar{\Lambda}$ fragmentation component compared to $\rho = 0.5$.

B. Subtraction of non-primary $\Lambda\bar{\Lambda}$ component

To estimate the non-primary $\Lambda\bar{\Lambda}$ contribution, we rely heavily on JETSET 7.4 Monte Carlo simulations. We use the following procedure to subtract $\Lambda\bar{\Lambda}$ (np) production in our search for an opposite-hemisphere, correlated, primary $\Lambda|\bar{\Lambda}$ ($q\bar{q}$) signal:

1. We plot the $\cos\theta_{\Lambda\bar{\Lambda}}$ distribution in both data and Monte Carlo simulations, with $\theta_{\Lambda\bar{\Lambda}}$ defined as the opening angle between Λ and $\bar{\Lambda}$.
2. We normalize the Monte Carlo $\Lambda\bar{\Lambda}$ yield in the forward hemisphere ($\cos\theta_{\Lambda\bar{\Lambda}} > 0$) to data, and subtract the result from data, for the full ($\cos\theta_{\Lambda\bar{\Lambda}}$) angular distribution. As noted previously, the match (absolutely normalized to the total number of Λ 's) between data and Monte Carlo simulations is satisfactory in the forward hemisphere ($\cos\theta_{\Lambda\bar{\Lambda}} > 0$), however there is an under-subtraction of events in the back hemisphere. This subtraction therefore results in an excess of back-to-back $\Lambda|\bar{\Lambda}$ events in data relative to Monte Carlo simulations.

C. Subtraction of $\Lambda_c|\bar{\Lambda}_c$ feeddown component from $\Lambda|\bar{\Lambda}$ yield

Based on the observed number of: a) $\Lambda_c|\bar{\Lambda}_c$, b) $\Lambda|\bar{\Lambda}$, and c) $\Lambda_c|\bar{\Lambda}$ in data, we can calculate the total number of $\Lambda|\bar{\Lambda}(c\bar{c})$ correlations, assuming that any Λ opposite a $\bar{\Lambda}_c$ is a Λ_c decay product (we discuss below two corrections to these assumptions). This is done by setting the probability that both charmed baryons in an $e^+e^- \rightarrow c\bar{c} \rightarrow \Lambda_c|\bar{\Lambda}_c$ decay to lambda baryons, relative to just one decaying to a lambda baryon, equal to the probability that one decays to a lambda, relative to the probability that neither decays to lambdas. Designating $\Lambda_c \rightarrow \Lambda$ as the inclusive Λ yield from Λ_c decay, this probability condition can be written as:

$$\frac{N(\Lambda_c \rightarrow \Lambda|\bar{\Lambda}_c \rightarrow \bar{\Lambda})}{N(\Lambda_c \rightarrow \Lambda|\bar{\Lambda}_c)} = \frac{N(\Lambda_c \rightarrow \Lambda|\bar{\Lambda}_c)}{N(\Lambda_c|\bar{\Lambda}_c)} \quad (2)$$

Monte Carlo simulations indicate that, with the kinematic requirements we impose on our candidate event sample, $(93 \pm 2)\%$ of the final state Λ 's produced in $\Lambda_c \rightarrow \Lambda$ are, indeed, opposite each other. Figure 5 shows the cosine of the opening angle between the final state Λ relative to the final state $\bar{\Lambda}$ in such feed-down events; as expected, the distribution peaks at $\cos\theta_{\Lambda\bar{\Lambda}} \rightarrow -1$. Thus, assuming that all the observed ($\Lambda|\bar{\Lambda}_c$) events result from $e^+e^- \rightarrow \Lambda_c|\bar{\Lambda}_c$ events in which $\Lambda_c \rightarrow \Lambda$ in the hemisphere opposite the $\bar{\Lambda}_c$, the number of “feed-down” ($\Lambda_c \rightarrow \Lambda|\bar{\Lambda}_c \rightarrow \bar{\Lambda}$) events can be determined from the above equation directly as: $N^2(\Lambda|\bar{\Lambda}_c)/N(\Lambda_c|\bar{\Lambda}_c) = 1671 \pm 221$.⁸ Using this value for the $\Lambda|\bar{\Lambda}(c\bar{c})$ background and subtracting the scaled MC background as described previously, we obtain, using the yields from Table I:

$$\begin{aligned} N(\Lambda|\bar{\Lambda}(q\bar{q})) &= \\ N(\Lambda|\bar{\Lambda})_{data} - N(\Lambda|\bar{\Lambda})_{MC} \times \frac{N(\Lambda|\bar{\Lambda})_{data}}{N(\Lambda|\bar{\Lambda})_{MC}} - N(\Lambda|\bar{\Lambda})(c\bar{c}) &= \\ 7362 - 6519 \times \frac{8425}{11395} - 1647 &= 872 \pm 288 \text{ events.} \end{aligned}$$

⁸Note that one must use only one charge conjugate in the numerator of this ratio ($N(\Lambda|\bar{\Lambda}_c) = 735.3$) to properly compare rates, per reconstructed $\bar{\Lambda}_c$.

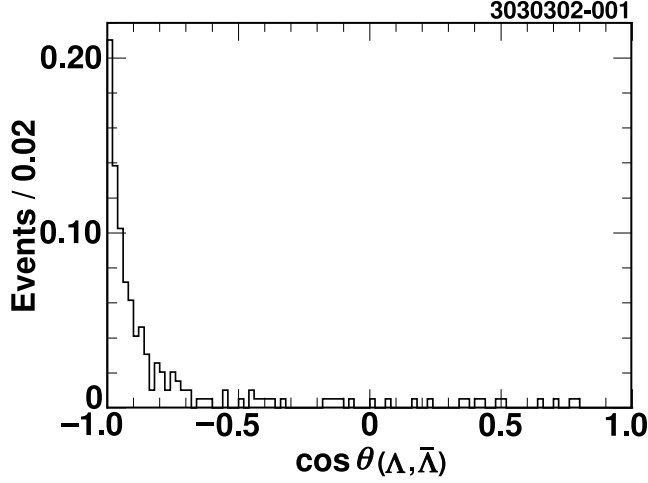


FIG. 5. Cosine of opening angle between $\bar{\Lambda}$ and Λ in $e^+e^- \rightarrow \Lambda_c \bar{\Lambda}_c \rightarrow \Lambda \bar{\Lambda}$ events, from Monte Carlo simulations. The distribution has been normalized to unity.

Thus, under the most pessimistic of background assumptions, we obtain a 3σ excess in our estimate of the primary, correlated $\Lambda|\bar{\Lambda}$ yield.

Some of the observed $\Lambda|\bar{\Lambda}_c$ events will arise from other sources, such as events in which a $\bar{\Lambda}$ baryon compensates the baryon number of the Λ_c ($D\bar{\Lambda}|\bar{K}\Lambda_c$, e.g). There will also be contributions from $(\Xi_c \rightarrow \Lambda)|\bar{\Lambda}_c$ and $(\Omega_c \rightarrow \Lambda)|\bar{\Lambda}_c$. The number of feed-down ($\Lambda_c \rightarrow \Lambda|\bar{\Lambda}_c \rightarrow \bar{\Lambda}$) calculated through the above prescription therefore yields an overestimate of the true feed-down contribution and therefore will yield a lower limit on correlated direct $\Lambda|\bar{\Lambda}$ production when the feed-down component is subtracted.

We correct our estimate of the $\Lambda\bar{\Lambda}(c\bar{c})$ background (1671 ± 221) with guidance from Monte Carlo simulations. In Monte Carlo simulations, for which the parentage of a given particle is known, we observe 169 ± 13 $\Lambda|\bar{\Lambda}$ events resulting from $\Lambda_c|\bar{\Lambda D}$ events. We estimate the number of ($\Lambda|\bar{\Lambda}_c$) events in our data sample resulting from $\Lambda_c|\bar{\Lambda D}$ events (and thus incorrectly attributed to ($\Lambda_c \rightarrow \Lambda|\bar{\Lambda}_c \rightarrow \bar{\Lambda}$)) by normalizing the number found in the Monte Carlo by the ratio of ($\Lambda\bar{\Lambda}_c + \Lambda_c\bar{\Lambda}$) (all angles) in data relative to Monte Carlo simulations:

$$(\Lambda_c|\bar{\Lambda D})_{data} = \frac{N(\Lambda_c\bar{\Lambda} + \Lambda\bar{\Lambda}_c)_{data}}{N(\Lambda_c\bar{\Lambda} + \Lambda\bar{\Lambda}_c)_{MC}} \times N(\Lambda_c|\bar{\Lambda D})_{MC} = \frac{249.4 \pm 26.2}{211.2 \pm 28.2} \times 169 = 199.5 \pm 34.$$

Using this value, we can now re-calculate the background we attribute to $\Lambda|\bar{\Lambda}(c\bar{c})$ as: $(N(\Lambda|\bar{\Lambda}_c) - 199.5)^2 / N(\Lambda_c|\bar{\Lambda}_c) = 1251 \pm 223$ events. This smaller background estimate implies a larger correlated signal yield:

$$\Lambda|\bar{\Lambda}(q\bar{q}) = 7362 - [6519 \times (8425/11395)] - 1251 = 1290 \pm 371 \text{ events.}$$

To better estimate the full effect we have to carry out the additional subtraction described in the following section.

D. Additional correction due to $\Lambda_c|\bar{\Lambda}_c$ production in Monte Carlo simulations.

Our subtraction of the non-primary component from Monte Carlo simulations has not been corrected for known $\Lambda|\bar{\Lambda}(c\bar{c})$ contributions in the simulation itself. The opposite-hemisphere $\Lambda|\bar{\Lambda}$ yield from Monte Carlo simulations given in Table I is therefore an overestimate of the non-primary component that we subtract out. Since the parent type in simulations is known, this correction can be made directly. We tabulate 477 ± 21.8 $\Lambda\bar{\Lambda}(c\bar{c})$ events contributing to our $\Lambda|\bar{\Lambda}$ sample in Monte Carlo simulations. The calculated yield of primary, correlated $\Lambda|\bar{\Lambda}$ events is now:

$$\Lambda|\bar{\Lambda}(q\bar{q}) = 7362 - [(6519 - 477) \times (8425/11395)] - 1251 = 1643 \pm 372.$$

E. Summary of Subtraction Procedure

Figure 6 displays the $\cos\theta_{\Lambda\bar{\Lambda}}$ distributions, as well as the subtraction procedure. Overlaid with the data $\cos\theta_{\Lambda\bar{\Lambda}}$ distribution is the Monte Carlo simulation. Applying the maximum possible $\bar{\Lambda}|\Lambda(c\bar{c})$ background estimate to the data distribution shown in Fig. 6, (i.e., not correcting for $\bar{D}\Lambda_c\bar{\Lambda}$ background in data or $\bar{\Lambda}|\Lambda(c\bar{c})$ in Monte Carlo simulations), we obtain the most conservative back-hemisphere excess of 872 ± 288 events (statistical errors only). Applying all corrections (as in the Figure), this excess is approximately doubled.

F. Search for correlated $\Lambda|\bar{\Lambda}$ excess relative to $\Lambda\bar{K}$

In our study of $\Lambda_c|\bar{\Lambda}_c$ correlations, we compared $\Lambda_c|\bar{\Lambda}_c$ to $\Lambda_c|\bar{D}$. In an analogous way, we shall attempt to compare $\Lambda|\bar{\Lambda}$ production relative to $\Lambda|K$ production. To normalize properly, we have compared the fractional production rate: $(\Lambda|\bar{\Lambda})/\bar{\Lambda}$ relative to $(\Lambda|K)/K$, where the denominator designates the total number of detected single-tag $\bar{\Lambda}$ (or K). This technique was used to search for evidence of correlated $\Lambda_c|\bar{\Lambda}_c$ production in our previous publication. While a \bar{D} tag always contains a primary quark, our K sample includes non-primary kaons, including those that are decay products of charmed hadrons.⁹ Although, in principle, the $D|K$ yield can provide some guidance as to the $c \rightarrow K$ rate, there are still considerable uncertainties resulting from the exact admixture of non-primary kaons relative to $c \rightarrow K$. What must be true, however, is that $s\bar{s} \rightarrow \Lambda|K$ events, in which the Λ and K both contain the primary quarks will result in only one flavor correlation; non-primary contributions can give rise to both $\Lambda|K$ and $\Lambda|\bar{K}$ correlations. Even in the absence of correlated primary $s\bar{s} \rightarrow \Lambda|K$ production, however, we still expect, because of strangeness conservation, Λ production in association with K (and not \bar{K}). For this analysis, we restrict ourselves to continuum data to exclude possible $B \rightarrow KX$ contributions. Yields are summarized in Table II.

We have searched for evidence of correlated production of $(\Lambda|\bar{\Lambda})$ by comparing the ratio of $(\Lambda|\bar{\Lambda})/\bar{\Lambda}$ to $(\Lambda|K)/K$; in each case, we can compare with “wrong-flavor” combinations $((\Lambda|\Lambda)/\Lambda$

⁹There are further complications arising from cases such as: $e^+e^- \rightarrow \Lambda\bar{\Lambda}(1420)$; $\bar{\Lambda}(1420) \rightarrow \bar{p}K^+$. In such cases, although observation of the Λ opposite the K^+ would be interpreted as a primary baryon-meson correlation, the true underlying event is a primary baryon-antibaryon correlation. We can safely neglect such instances as long as the Monte Carlo simulation is producing such events at approximately the correct rate.

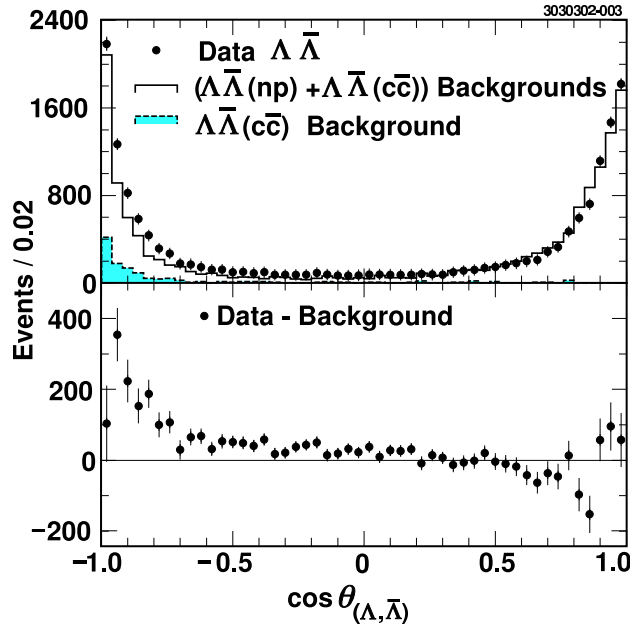


FIG. 6. $\cos \theta_{\Lambda \bar{\Lambda}}$ distribution for data (\bullet) with total background overlaid (unshaded histogram). The Monte Carlo $\cos \theta_{\Lambda \bar{\Lambda}}$ distribution is corrected for the expected $(\Lambda_c \rightarrow \Lambda | \bar{\Lambda}_c \rightarrow \bar{\Lambda})$ contribution (normalization obtained from data, with the shape taken from Monte Carlo simulations), applying all corrections cited in the text. That total background distribution has been normalized to the data in the region $\cos \theta_{\Lambda \bar{\Lambda}} > 0$, then subtracted from the data distribution. The bulk of the background histogram is due to $\Lambda | \bar{\Lambda}$ (np) production. The component of the total background due exclusively to $\Lambda | \bar{\Lambda}$ ($c\bar{c}$) is shown as the shaded histogram. The final, background-subtracted (all corrections applied) data excess is shown in the lower panel.

TABLE II. Kaon-Lambda correlation yields in data vs. Monte Carlo simulations. The data are drawn from the same sample as for the previous Table. Derivation of final results is discussed in detail in the text. No fake subtractions have been applied to the quoted charged kaon yields.

	Data	Monte Carlo
K^- (Continuum, ONLY)	325427 ± 570	1130987 ± 1064
K^+ (Continuum, ONLY)	330010 ± 574	1149240 ± 1072
(ΛK^+)	2009.5 ± 50.6	9426.3 ± 106.0
(ΛK^+)	738.8 ± 30.5	2598.4 ± 55.2
(ΛK^-)	979.6 ± 38.7	3933.6 ± 75.4
(ΛK^-)	344.8 ± 23.2	899.4 ± 37.6
$(\Lambda K^+)/K^+ (\times 10^{-3})$	6.1 ± 0.1	8.2 ± 0.1
$(\Lambda K^+)/K^+ (\times 10^{-3})$	2.2 ± 0.1	2.3 ± 0.1
$(\Lambda K^-)/K^- (\times 10^{-3})$	3.0 ± 0.1	3.5 ± 0.1
$(\Lambda K^-)/K^- (\times 10^{-3})$	1.1 ± 0.1	0.8 ± 0.1
$\mathcal{D}_{K^+} (\times 10^{-3})$	3.9 ± 0.2	5.9 ± 0.1
$\mathcal{D}_{K^-} (\times 10^{-3})$	2.0 ± 0.1	2.7 ± 0.1
\mathcal{S}	8.8 ± 0.3	3.8 ± 0.1

and $(\Lambda|\bar{K})/\bar{K}$), as well as same hemisphere combinations, as estimates of the fake-kaon and non-primary components. Contributions to ΛK^+ will arise from: i) correlated, primary production, ii) weak decays of charmed hadrons in $\Lambda_c|\bar{D}$ events, iii) compensation of non-primary strange quark production, and iv) fake kaons. Contributions to ΛK^- will arise primarily from non-primary and fake kaons. In order to isolate correlated primary production, we therefore define, for both Monte Carlo simulations as well as data, the subtracted, normalized fractions: $\mathcal{D}_{K^+} \equiv (\Lambda|K^+)/K^+ - (\Lambda K^+|)/K^+$ and $\mathcal{D}_{K^-} \equiv (\Lambda|K^-)/K^- - (\Lambda K^-|)/K^-$. We also define a signal ratio \mathcal{S} , in analogy to our previous publication $\mathcal{S} \equiv \frac{(\Lambda|\bar{\Lambda} - \Lambda|\bar{\Lambda}(c\bar{c}))/\Lambda}{\mathcal{D}_{K^+} - \mathcal{D}_{K^-}}$. Note that, in constructing this ratio, we subtract the contributions to the $\Lambda|\bar{\Lambda}$ enhancement from $\Lambda_c \rightarrow \Lambda|\bar{\Lambda}_c \rightarrow \bar{\Lambda}$ to ensure that any observed enhancement is not due to the previously measured $\Lambda_c|\bar{\Lambda}_c$ enhancement. We find $\mathcal{S}(data) = 8.77 \pm 0.26$, compared with $\mathcal{S}(MC) = 3.79 \pm 0.08$ (statistical errors only). This is consistent with an enhancement of correlated primary baryon-antibaryon production compared to correlated primary baryon-meson production. We note that the (unevaluated) systematic uncertainties in this analysis are expected to be considerable, as indicated by the discrepancy in the \mathcal{D}_{K^+} values between data and Monte Carlo simulations (suggesting a greater likelihood of strangeness conservation to occur by production of mesons vs. baryons in simulations), as well as the discrepancy in the \mathcal{D}_{K^-} values (suggesting different fake rates in the simulation compared to the data). Because of the large systematic errors associated with this exercise, the significance of the difference between \mathcal{S} (data) and \mathcal{S} (Monte Carlo) cannot be simply evaluated on the basis of the statistical errors. This exercise is to be viewed only as a check of the primary $\Lambda|\bar{\Lambda}$ production enhancement discussed in subsections III A through III E.

G. Comparison to correlated $\Lambda_c|\bar{\Lambda}_c$ production

In principle, one might hope to compare the yield of correlated $\Lambda|\bar{\Lambda}$ production to that of $\Lambda_c|\bar{\Lambda}_c$. Quantitatively, one could compare correlated primary baryon production for charmed vs. non-charmed baryons, via the ratio: $N(\Lambda_c|\bar{\Lambda}_c)/\epsilon_{\Lambda_c}^2/c\bar{c}$ relative to: $N(\Lambda|\bar{\Lambda})/\epsilon_{\Lambda}^2/q\bar{q}$. The efficiency factors ϵ include both the reconstruction efficiency in each case, as well as the fraction of the momentum spectrum accepted, given the minimum momentum requirements in each case ($p > 2.3$ GeV/c for the Λ_c analysis vs. $p > 1.0$ GeV/c in the Λ analysis).¹⁰ What is unknown in the case of the Λ is what fraction of $u\bar{u}$ vs. $d\bar{d}$ vs. $s\bar{s}$ evolve into $p|\bar{p}$, $n|\bar{n}$, $\Lambda|\bar{\Lambda}$, $\Lambda|\bar{\Sigma}^+$, $\Lambda|K^+\bar{p}$, etc. Nevertheless, ignoring such unknowns, and using efficiencies ϵ_{Λ} and ϵ_{Λ_c} from Monte Carlo simulations ($\epsilon_{\Lambda} \sim 0.091$ and $\epsilon_{\Lambda_c} \sim 0.022$), we expect to observe ~ 5300 $\Lambda|\bar{\Lambda}$ correlations, scaling from the observed $\Lambda_c|\bar{\Lambda}_c$ correlations. We observe $\approx 20\%$ of the expected value, consistent with a model in which primary baryon-antibaryon correlations in $s\bar{s}$ events are populated equally by $\Lambda|\bar{\Sigma}$, $\Lambda|\bar{\Lambda}$ and $\Sigma|\bar{\Sigma}$, with very little contribution from $e^+e^- \rightarrow u\bar{u}$ and $e^+e^- \rightarrow d\bar{d}$. Unfortunately, a) photon-finding ($\Sigma \rightarrow \Lambda\gamma$ or $\Sigma^+ \rightarrow p\pi^0$) systematics, b) substantially lower signal-to-noise ratios compared to $\Lambda \rightarrow p\pi^-$, c) reduced statistics, and d) the necessity to reconstruct a secondary vertex from a single charged track plus neutrals ($\Sigma^+ \rightarrow p\pi^0$, e.g.) make the Σ correlation analyses considerably more difficult than the analysis described herein.

IV. SYSTEMATICS

Since this analysis relies crucially on the ability of the Monte Carlo simulation to model angular correlations in the data, it is important that related kinematic parameters be checked. To verify that JETSET models two-particle opening angle ($\cos\theta_{+-}$) distributions adequately, we have compared Monte Carlo expectations to the data for the opening angle distribution between oppositely signed tracks (Figure 7). For six different minimum momentum requirements, the Monte Carlo simulation is observed to model the data quite well.

To examine the dependence of our result on the minimum momentum requirement, we have analyzed the $\Lambda|\bar{\Lambda}$ excess (data - background) using different minimum momentum restrictions on our Λ sample. We find that the match between data and simulation, for the normalized same-hemisphere yield $(\Lambda|\bar{\Lambda})/\Lambda$, remains excellent for $p > 0.5$ GeV/c (0.0164 ± 0.0001 for data vs. 0.0168 ± 0.0001 for simulation) as well as for $p > 1.2$ GeV/c (0.0092 ± 0.0001 for data vs. 0.0091 ± 0.0001 for simulation). With all corrections applied, opposite-hemisphere excesses are still observed for $p_{\Lambda} > 0.5$ GeV/c (3306 ± 543 events) and $p_{\Lambda} > 1.2$ GeV/c (865 ± 283 events).

Although the minimum momentum requirement ($p_{\Lambda} > 1.0$ GeV/c) should be highly efficient at removing backgrounds from $B \rightarrow \Lambda X$, there is still some residual contamination of our single-tag Λ and our double-tag $\Lambda|\bar{\Lambda}$ sample from $\Upsilon(4S)$ decays. Inspection of Table I indicates that these may represent $\sim 3\%$ corrections to both the single-tag and double-tag $\Lambda|\bar{\Lambda}$ samples; our yields indicate that the contamination to the same-hemisphere $\Lambda|\bar{\Lambda}$ yield is considerably less. Therefore, making such corrections explicit would have the effect of modifying our ratios and our corrected yields by, at most, $\sim 3\%$.

¹⁰ One might argue that since, in the scaled variable $\beta = p/m$, the two requirements are approximately equivalent, the acceptances are also comparable.

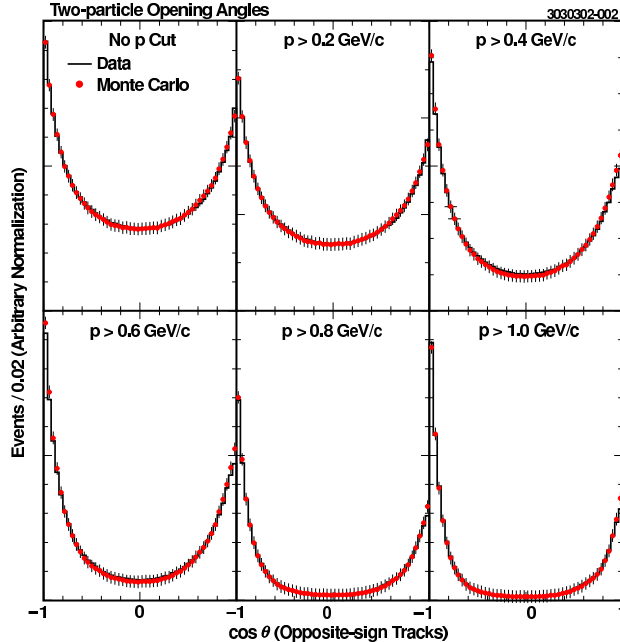


FIG. 7. $\cos(\theta)_{+-}$, defined as the opening angle distribution for all oppositely-signed charged track pairs, for data (+) vs. JETSET 7.4 Monte Carlo simulations (-). The histograms have been normalized to equal areas.

The analysis would obviously be cleaner if the parent of each Λ could be unambiguously identified. Because it is not possible to definitively distinguish Λ baryons which contain primary quarks from non-primary baryons, the extraction of the correlated, primary $\Lambda|\bar{\Lambda}$ signal is inherently Monte Carlo dependent. Only in the previous case of $\Lambda_c|\bar{\Lambda}_c$ production could one conclusively distinguish first-rank from higher-rank baryon production (since higher-rank Λ_c production, at our energies, is expected to be zero). In principle, one might hope to separate primary Λ production from non-primary Λ production through several techniques; each technique is, however, fraught with its own particular difficulties. Measurements such as three-fold $\bar{\Lambda}\bar{D}\Lambda_c$ correlations or $e^+e^- \rightarrow \gamma\Lambda\bar{\Lambda}X$ production, in which the (initial state radiation) photon has sufficiently high energy to exclude $\Lambda_c \rightarrow \Lambda X$ production, can help us assess, e.g., the contribution to Λ production from charmed baryon decays, but cannot define the presence or absence of a correlated primary signal. In the CLEO-c era ($\sqrt{s} \sim 4$ GeV), the limited phase space should make this measurement considerably simpler.

V. $\Xi|\bar{\Xi}$ CORRELATIONS

In principle, $(\Xi|\bar{\Xi})$ pairs may be used to further refine our understanding of primary quark-antiquark production and may, e.g., be used as a discriminant between different [12] models of baryon-antibaryon correlations. Examining $\Lambda\pi^-$ invariant mass combinations, we have observed a small, but statistically significant signal for $\Xi|\bar{\Xi}$ correlations (Figure 8). Unfortunately, the limited signal size is insufficient to attempt to measure primary correlated $\Xi|\bar{\Xi}$ production. Nevertheless, it is of interest to compare the yield of $\Xi^+\Xi^-$, normalized to the total number of charged cascades: $\Xi^+\Xi^-/(\Xi^+ + \Xi^-)$, relative to the corresponding value for lambda baryons: $\Lambda\bar{\Lambda}/(\Lambda + \bar{\Lambda})$. Loosening

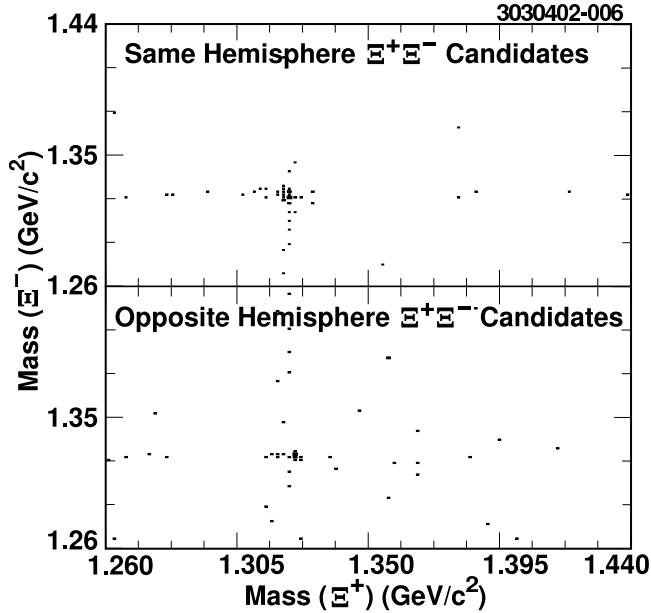


FIG. 8. Same hemisphere and opposite hemisphere $\Xi^+\Xi^-$ candidate invariant mass distributions ($p_{\Xi} > 0.5$ GeV/c). The correlation is most pronounced in the same hemisphere.

our minimum momentum requirement to 0.5 GeV/c, we find 14537 ± 135 total ($\Xi^+ + \Xi^-$), an opposite-hemisphere yield ($\Xi^+|\Xi^-$) = 13.0 ± 3.9 , and a same hemisphere yield ($\Xi^+\Xi^-$) = 21.2 ± 5.1 . Correspondingly, we obtain $(\Xi^+\Xi^-)/(\Xi^+ + \Xi^-) = (1.5 \pm 0.4) \times 10^{-3}$ for same-hemisphere cascades, vs. $(\Lambda\bar{\Lambda})/(\Lambda + \bar{\Lambda}) = (23 \pm 0.4) \times 10^{-3}$ for same-hemisphere lambdas. For opposite hemisphere baryon-antibaryon correlations, the corresponding numbers are $(0.9 \pm 0.3) \times 10^{-3}$ and $(28 \pm 0.6) \times 10^{-3}$. In contrast to di-lambda production, di-cascade production favors (albeit with small statistics) same- rather than opposite-hemisphere production. Normalized to the total number of baryons, the di-cascade rate (integrated over all angles) is apparently suppressed relative to the di-lambda rate. This is consistent with a model in which cascade and lambda production is dominated by light quark popping; in such a picture, Ξ^- suppression is therefore a direct consequence of strangeness suppression.

VI. SUMMARY

Under conservative assumptions, we observe a $\sim 3\sigma$ (872 ± 288) excess of opposite-hemisphere $\Lambda|\bar{\Lambda}$ production in data compared to the expectations of the JETSET 7.4 event generator combined with the full simulation of our detector, and after accounting for feeddown production of $\Lambda\bar{\Lambda}$ from charmed baryons. With appropriate corrections applied, this excess increases to (1643 ± 372) events. These results are consistent with enhanced correlated, primary $\Lambda|\bar{\Lambda}$ production, of the type observed previously in $\Lambda_c|\bar{\Lambda}_c$ correlations. However, we stress the inherent Monte Carlo dependence of this conclusion (not present in the $\Lambda_c|\bar{\Lambda}_c$ correlation analysis [5]), and that the complete parameter space of the event generator has not been fully explored. Data-taking planned for CLEO-c at $D|\bar{D}$ threshold should be able to more definitively measure such $\Lambda|\bar{\Lambda}$ correlations, in a considerably less Monte Carlo-dependent manner.

VII. ACKNOWLEDGMENTS

We gratefully acknowledge the effort of the CESR staff in providing us with excellent luminosity and running conditions. M. Selen thanks the PFF program of the NSF and the Research Corporation, and A.H. Mahmood thanks the Texas Advanced Research Program. This work was supported by the National Science Foundation, and the U.S. Department of Energy.

REFERENCES

- [1] T. Sjostrand, LUND 7.4, CERN Report No. CERN-TH-6488-92, 1992; T. Sjostrand, Comp. Phys. Comm. **82** (1994) 74-89, T. Sjostrand, “PYTHIA 5.7 and JETSET 7.4 Physics and Manual”, hep-ph/9508391.
- [2] The DELPHI Collaboration, P. Abreu *et al.*, Phys. Lett. **B318**, 249 (1993).
- [3] The ALEPH Collaboration, Z. Buskolic *et al.*, Z. Phys. **C64** 361 (1994).
- [4] The OPAL Collaboration, G. Abbiendi *et al.*, Eur. Phys. J. **C13**, 185 (2000).
- [5] The CLEO Collaboration, A. Bornheim *et al.*, Phys. Rev. **D63**, 112003 (2001).
- [6] R. Brun *et al.*, “GEANT3 Users Guide,” CERN DD/EE/84-1 (1987).
- [7] The CLEO Collaboration, Y. Kubota *et al.* , Nucl. Instrum. Methods Phys. Res. A **320**, 66 (1992).
- [8] T. S. Hill *et al.*, Nucl. Inst. Meth. Phys. Res., Sec. A **A418**, 32 (1998).
- [9] D. Peterson *et al.*, Nucl. Phys B (Proc Supp) **54B**, 31 (1997).
- [10] The CLEO Collaboration, R. Ammar *et al.*, Phys. Rev. **D62**, 092007 (2000).
- [11] The CLEO Collaboration, D. Jaffe *et al.* Phys. Rev. **D62**, 072005 (2000).
- [12] A. Casher, H. Neuberger and L. Susskind, Phys. Rev. **D10** 732 (1974); B. Andersson “The Lund Model”, Cambridge University Press (1998) page 241.